SUB-LUMINOUS γ -RAY PULSARS

R.W. Romani, M Kerr, H.A. Craig, S Johnston, Ismaël Cognard, D.A. Smith

▶ To cite this version:

HAL Id: in2p3-00655793
https://hal.in2p3.fr/in2p3-00655793

Submitted on 13 Mar 2015

SUB-LUMINOUS γ-RAY PULSARS

R. W. ROMANI[1], M. KERR[1,6], H. A. CRAIG[1], S. JOHNSTON[2], I. COGNARD[3,4], AND D. A. SMITH[5]
[1] Department of Physics, Stanford University, Stanford, CA 94305, USA; rwr@astro.stanford.edu
[2] Australia Telescope National Facility, CSIRO, Epping, NSW 1710, Australia
[3] Laboratoire de Physique et Chimie de l'Environnement, LPCE UMR 6115 CNRS, 45071 Orléans Cedex 02, France
[4] Station de radioastronomie de Nançay, Observatoire de Paris, CNRS/INSU, 18330 Nançay, France
[5] Centre d'Etudes Nucléaires de Bordeaux Gradignan, Université Bordeaux 1, CNRS/IN2p3, 33175 Gradignan, France

ABSTRACT

Most pulsars observed by the *Fermi* Large Area Telescope have γ-ray luminosities scaling with spin-down power $\dot{E}$ as $L_\gamma \approx (\dot{E} \times 10^{33} \, \mathrm{erg \, s^{-1}})^{1/2}$. However, there exist one detection and several upper limits an order of magnitude or more fainter than this trend. We describe these "sub-luminous" γ-ray pulsars and discuss the case for this being an orientation effect. Of the 12 known young radio pulsars with $\dot{E} > 10^{34} \, \mathrm{erg \, s^{-1}}$ and $d \leqslant 2$ kpc several are substantially sub-luminous. The limited available geometrical constraints favor aligned geometries for these pulsars, although no one case for alignment is compelling. In this scenario GeV emission detected from such sub-luminous pulsars can be due to a lower altitude, lower-power accelerator gap.

Key words: gamma rays: stars – pulsars: general

Online-only material: color figures

1. INTRODUCTION

The Large Area Telescope (LAT) on the *Fermi* satellite has now detected over 75 spin-powered pulsars (Abdo et al. 2010a). Among the ≈50 non-recycled energetic pulsars, there is a clear trend for γ-ray "efficiency" to increase with decreasing spin-down power $\dot{E}$, giving a heuristic γ-ray luminosity

$$L_{\gamma,\mathrm{heu}} \approx (\dot{E} \times 10^{33} \, \mathrm{erg \, s^{-1}})^{1/2}. \tag{1}$$

This is a natural result for models where the emission is produced by a Goldreich–Julian current of charges passing through a characteristic potential drop (Harding 1981; Arons 1996). Of course, energy conservation limits $L_\gamma < \dot{E}$, and as $\dot{E}$ decreases, the star is unable to maintain the potential drop, leading to a "death zone" below $\dot{E} \approx 10^{33}$–$10^{34} \, \mathrm{erg \, s^{-1}}$ where this process starts to turn off. This is portrayed in Figure 5 of Abdo et al. (2010a), where most energetic pulsars lie between Equation (1) and unit efficiency. Only two young pulsars in that plot lie significantly below the $L_{\gamma,\mathrm{heu}}$ line: PSR J0205+6449, where a small inferred distance places it just below this value and PSR J0659+1414 (to be discussed in this paper) which is ∼20× less luminous. Thus, independent of its physical validity, Equation (1) forms an effective lower luminosity envelope to the bulk of the observed pulsar sample.

Estimates of L_γ suffer two complications. The first is the source distance; for most LAT pulsars we have only distance estimates based on the pulsar dispersion measure (DM). DM modeling (Cordes & Lazio 2002, hereafter CL02) is believed to provide statistically useful estimates of pulsar distances, with a scatter of ≈30% about independent distance estimates, although typical errors for nearby pulsars may be as large as 60% (see Deller 2009). DM distances are certainly not reliable for individual objects, and it appears (Abdo et al. 2010a) that they may be especially poor for the young, energetic LAT pulsars. This is likely since the sample is nearby and associated with regions of active star formation where the excess ionized gas may significantly perturb the DMs. About one-third of the LAT

pulsars are found directly in the γ-ray data through so-called blind searches (Abdo et al. 2009; Saz Parkinson et al. 2010); most of these lack radio detections and so do not even have DM distance estimates. The second complication is the conversion from the observed energy flux F_E along the Earth line of sight to the true-sky-averaged luminosity

$$L_\gamma = 4\pi f_\Omega F_E D^2. \tag{2}$$

Watters et al. (2009) and Romani & Watters (2010, RW10) have estimated "flux conversion factors" f_Ω for this correction for a variety of pulsar models and viewing geometries. For most of the observed pulsars, f_Ω should be in the range 0.7–1.3, although some lower $\dot{E}$ pulsars, especially γ-selected objects (Watters & Romani 2011), may have f_Ω as small as 0.1 for "outer gap" (OG) geometries.

However, there are a handful of pulsars whose observed luminosity or limit fall an order of magnitude or more *below* $L_{\gamma,\mathrm{heu}}$. In spite of the uncertainties just discussed we can make a case that they are truly sub-luminous. There are three possible interpretations. The first is that the γ-ray radiation is beamed away from the Earth line of sight (or equivalently $f_\Omega > 10$). The second is that some particular physical property of the pulsar prevents them from producing the bright high-altitude γ-ray emission typical of other energetic pulsars. The third is that the DM distance is especially poor and the pulsar is much more distant than estimated. We test here the first possibility, that γ-ray beaming explains the low observed fluxes of some nearby energetic pulsars. We also comment briefly on the possibility that objects with detected luminosities $\ll L_{\gamma,\mathrm{heu}}$ may be probing an emission component different to the powerful high-altitude gap emission which apparently dominates the bulk of the LAT-detected pulsars.

2. THE SUB-LUMINOUS PULSAR CANDIDATES

To find sub-luminous pulsars, we measure the DC (unpulsed) flux at the positions of nearby ($d \leqslant 2$ kpc), energetic ($\dot{E} > 10^{34} \, \mathrm{erg \, s^{-1}}$) non-recycled radio pulsars selected from the ATNF pulsar catalog (Manchester et al. 2005). There are 12 such

---

[6] Einstein Fellow.

Table 1
Young Local, Energetic Radio Pulsars: DC Fluxes and Geometry Constraints

Name	$\log(\dot{E})$ (erg s^{-1})	$\log(\tau_c)$ (yr)	d[c] (kpc)	$F_{E,>0.1\,\mathrm{GeV}}$ (10^{-12} erg cm^2 s^{-1})	W_{10} (deg)	W_1 (deg)	$\Delta\phi_{\mathrm{P.A.}}$ (deg)[d]	h_{LC}	B_{LC} (kG)	Reference [e]
J0358+5413	34.65	5.75	$1.04^{+0.21}_{-0.16}$	< 12.8	38.9	56	13.5	0.059	2.1	1
J0534+2200[b]	38.66	2.98[f]	2.0	$1828.^{+3.}_{-21.}$					980.	
J0538+2817	34.69	4.60[f]	$1.30^{+0.22}_{-0.16}$	< 4.5	55.4	92	35.0	0.153	2.3	2
J0633+1746[a,b]	34.52	5.53	$0.25^{+0.12}_{-0.06}$	$4340.^{+34.}_{-29.}$	. . .	. . .	. . .	. . .	1.2	
J0659+1414[b]	34.58	5.05	$0.288^{+0.033}_{-0.027}$	$41.6^{+6.8}_{-5.8}$	31.3	54	13.9	0.061	0.8	3
J0745−5353	34.04	6.10	0.25	< 0.98	34.9	61	4.0	0.017	0.8	Unpublished
J0834−4159	34.99	5.64	1.66	< 5.6	24.0				3.9	
J0835−4510[b]	36.84	4.05	$0.287^{+0.019}_{-0.017}$	$9466.^{+3.}_{-3.}$	16.9	27	4.2	0.018	45.	4
J0857−4424	34.42	5.35	1.94	$13.1^{+6.6}_{-6.2}$	18.7				0.8	
J1057−5226[b]	34.48	5.73	0.72	$294.^{+9.5}_{-8.2}$	31.0				1.3	
J1722−3712	34.52	5.53	1.85	$12.8^{+10.0}_{-8.5}$	13.3	22	12.0	0.052	1.2	Unpublished
J1740+1000	35.36	5.06	1.24	< 2.9	42.5	71	28.0	0.122	4.7	Unpublished
J1932+1059[a]	33.59	6.49	$0.361^{+0.010}_{-0.009}$	< 2.9	19.1	55	4.5	0.020	0.4	4
J2043+2740[b]	34.75	4.08[f]	1.80	$12.7^{+3.6}_{-3.0}$	16.6	32	8.0	0.035	3.7	5

Notes.
[a] Comparison pulsars, not members of the uniform radio loud, $\dot{E} > 10^{34}$ erg s^{-1}, $d \leqslant 2$ kpc set.
[b] *Fermi*-LAT pulsed detection.
[c] Parallax distances from the Australia Telescope National Facility database. CL02 DM distances (without errors). Classical Crab kinematic distance.
[d] $\Delta\phi_{\mathrm{P.A.}}$ measured from the W_{10} pulse center.
[e] Reference for the polarization profile used to fit the pulse widths, offsets, and polarization sweeps: 1, Gould & Lyne 1998; 2, von Hoensbroech & Xilouris 1997; 3, Everett & Weisberg 2001; 4, Johnston et al. 2005; 5, Noutsos et al. 2011.
[f] Age of the associated supernova remnant; τ_c is larger, implying initial spin period $P_0 \sim P$.

objects (Table 1 also includes two comparison objects). Since the LAT has detected several pulsars, especially millisecond pulsars, in the $\sim 10^{33}$–10^{34} erg s^{-1} boundary of the "death zone" we also consider the well-studied nearby $\dot{E} = 10^{33.6}$ erg s^{-1} pulsar PSR J1932+1059 (B1929+10), which has a low-LAT flux limit. Finally, for comparison we include Geminga (J0633+1746), a nearby γ-selected pulsar with an *Hubble Space Telescope* parallax measurement. We should note that this distance cutoff is somewhat arbitrary; for example, PSR J1747−2958 with a CL02 distance of 2.01 kpc is a LAT pulsed detection.

To measure the unpulsed fluxes, we use 24 months of LAT data (2008 August 4–2010 August 4) and the P6_V11 instrument response function, a refinement to previous analyses reflecting improved understanding of the point-spread function and effective area (A. A. Abdo et al. 2011, in preparation). "Diffuse-class" events were selected from good runs with rocking angle $<52°$, reconstructed energies $-0.75 < \log(E_\gamma/\mathrm{GeV}) < 2$, and a reconstructed zenith angle $<100°$. The list of point sources used in the background model is drawn from a preliminary version of the two-year *Fermi* catalog. The analysis used an updated version of the model for the diffuse background—Galactic, extragalactic, and residual cosmic rays—that is being prepared for publication by the LAT team. Like the model used for the 1FGL catalog (Abdo et al. 2010b) it is based on fitting templates for the diffuse emission to the LAT data.

For each pulsar we assume an exponentially cutoff spectrum $dN/dE = N_0 (E/\mathrm{GeV})^{-\Gamma} \exp(-E/E_c)$. For the bright LAT-detected pulsars (marked [b] in the table) we allow E_c and Γ to vary in the fits; the results are consistent with parameters quoted in Abdo et al. (2010a). For the other pulsars we set these parameters to values determined from an empirical fit to detected LAT pulsars (RW10): $\Gamma = -4.1 + 0.156 \log_{10}\dot{E}$ and $E_c/\mathrm{GeV} = -0.45 + 0.71 \log_{10} B_{\mathrm{LC}}$, with B_{LC} the magnetic field measured at the pulsar's light cylinder. We evaluate the likelihood for N_0 at the known pulsar position using "pointlike," a binned likelihood analysis tool (Kerr 2010), and using a Bayesian approach with

a uniform prior we integrate the likelihood to 97.5% to obtain a 2σ upper limit on the flux. For sources with apparent DC emission, we determine the corresponding 95% range for the measured N_0. For comparison with results in Abdo et al. (2010a) these measurements and upper limits are then converted to $E > 0.1$ GeV fluxes using the model spectra. The uncertainties reported for the measured fluxes are statistical only; additional systematic error arises from uncertainty in the effective area of the LAT (about 20% below 1 GeV, 10% at 1–10 GeV, and 30% above 10 GeV) and the structure of the diffuse background. Systematic uncertainties in the upper limits stem primarily from uncertainty in the background model and are comparable in magnitude to those associated with the assumed beaming factor discussed below.

Our study gives six candidate sub-luminous pulsars (marked in bold). Three in the uniform sample (plus PSR J1932+1059 = B1929+10) have parallax distance measurements. These are particularly important as the parallax constraints control a major factor in the luminosity uncertainty, allowing us to probe the effects of beaming geometry and gap emissivity. For the others we must rely at present on the DM distance estimates. These pulsars are displayed in Table 1 and Figure 1. Figure 1 also shows several other nearby non-recycled LAT-detected pulsars, highlighting the separation of our sub-luminous set from this sample. For this figure we have assumed $f_\Omega = 1$ for all pulsars. The plotted luminosity errors are dominated by the distance uncertainties, but do include the statistical flux errors. Of course, systematic errors and non-unity f_Ω may add additional uncertainty for individual pulsars.

3. EXTERNAL ANGLE CONSTRAINTS

For simple dipole models (e.g., the OG model) the pulse profile and the expected radiation on the Earth line of sight are determined by the magnetic inclination angle α and the viewing angle ζ. If these angles are known, we can predict γ-ray pulse
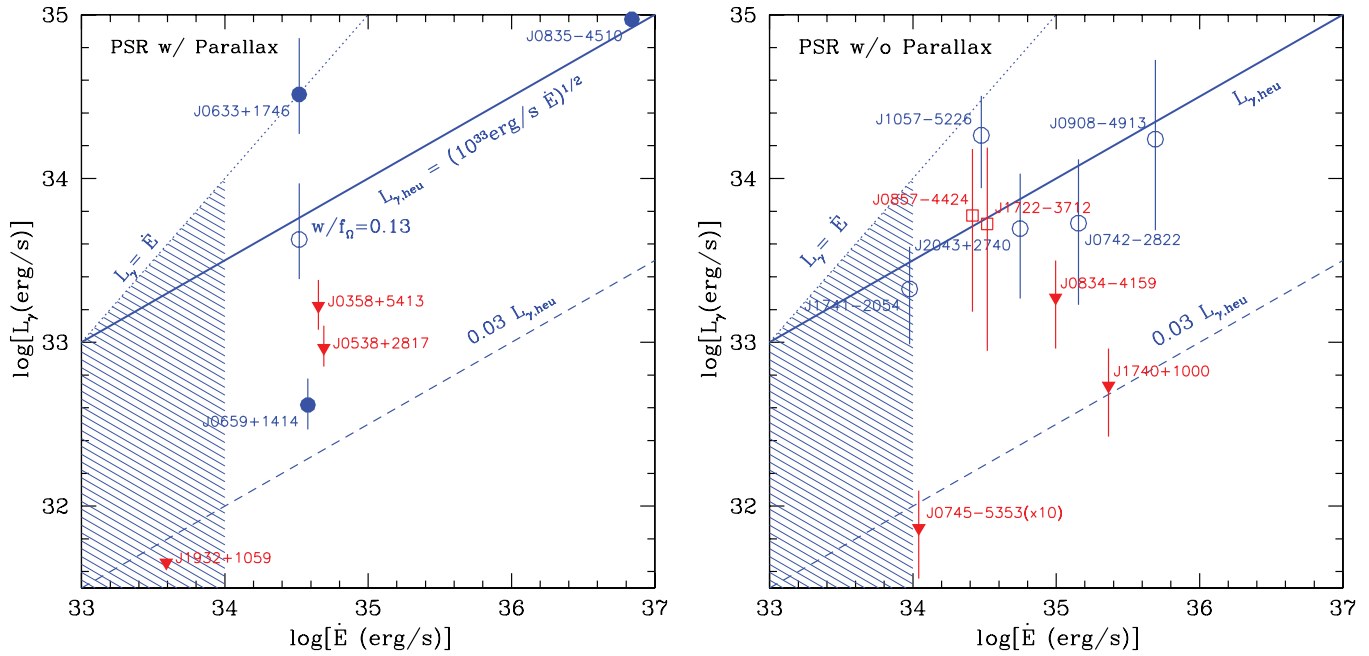
Figure 1. Spin-down-luminosity plane for energetic pulsars, with the heuristic luminosity trend, which saturates somewhere in the "death zone" (shaded). Unpulsed (DC) $E > 0.1$ GeV luminosities or limits are plotted, assuming $f_\Omega = 1$ (the RW10 $f_\Omega = 0.13$ point for Geminga is also shown). Left: objects with parallax distance measurements. The 95% error bars for LAT-detected objects (circles) include the flux imprecision, but are dominated by the parallax uncertainty. For the 95% upper limits (triangles), the error flags represent the parallax uncertainty. Right: objects with DM-estimated distances. Circles: the DC luminosities for radio pulsars with LAT pulse detections; squares: LAT DC detections (this paper); triangles: DC upper limits. All error bars include an assumed 30% DM distance uncertainty. For a few of the fainter LAT detections flux uncertainties contribute significantly. For PSR J0745−5353 the luminosity at the DM-estimated distance is 10× lower than the point shown.

(A color version of this figure is available in the online journal.)

profiles and fluxes for specific models and correct observations to the true L_γ. Unfortunately, these are poorly known in many cases.

3.1. Radio Polarization Data

The sub-luminous candidates treated here are known radio pulsars, so the magnetic impact angle $\beta = \zeta - \alpha$ is believed to be small. In the context of the rotating vector model (Radhakrishnan & Cooke 1969) radio polarization data can constrain the viewing angles. In most cases, the small range of phase illuminated by the radio pulse allows only an estimate of the magnetic impact angle

$$\beta = \zeta - \alpha \approx \sin^{-1}[\sin\alpha/(d\Psi/d\phi)_{\max}], \qquad (3)$$

where the maximum rate of the polarization position angle (P.A.) sweep $\Psi(\phi)$ occurs at $\phi_{d\psi,\max}$, near the closest approach to the magnetic axis. Here the sign of the sweep is meaningful, determining whether the line of sight is closer to or farther from the positive rotation axis than the observed magnetic pole (at inclination α). Occasionally, when the radio pulse is very broad or when the pulse profile presents an inter-pulse, the radio polarization can make meaningful estimates of both α and ζ, from fits to the full polarization sweep

$$\tan(\Psi + \Psi_0) = \frac{\sin\alpha \sin(\phi - \phi_0)}{\sin\zeta \cos\alpha - \cos\zeta \sin\alpha \cos(\phi - \phi_0)}, \qquad (4)$$

where the polarization has the absolute P.A. Ψ_0 at ϕ_0. Keith et al. (2010) have recently presented several examples of constraining fits of Equation (4) to high-quality polarization data. As described by Everett & Weisberg (2001), while nearly

all authors fit to Equations (3) and (4), given the standard astronomical convention of P.A. measurement (increasing N through E) these equations are inconsistent with pulsar angles increasing from the positive spin axis (the "rotating vector model (RVM) convention problem"). To be consistent, one must actually use $\alpha_{EW01} = \pi - \alpha_{RVM}$ and $\beta_{EW01} = -\beta_{RVM}$. Usually this correction is only a formality, but as fits to the γ-ray emission improve, including details of sweep-back and magnetospheric currents, the signs can be important. Thus, in the figures and discussion to follow, we convert all "RVM"-fit angles to the consistent Everett & Weisberg (2001) convention; we encourage future workers to do the same.

Other phenomenological constraints may be extracted from the radio data. For example, radio emission is generally believed to be produced within the "open zone" above the polar cap. For a static aligned dipole the half-opening angle covered by this radio beam is

$$\rho = 3/2h_{LC}^{1/2} \qquad (5)$$

radians for modest emission altitudes $h_{LC} = 2\pi h/Pc$. If the observed radio pulse fills this cone we can write h_{LC} in terms of the pulse width $W \approx 2\rho$

$$h_{LC} = 4/9 A\cos^2[\cos\alpha \cos\zeta + \sin\alpha \sin\zeta \cos(W/2)], \qquad (6)$$

if the radio emission does not fill the open zone this provides a lower limit for the emission height. It has also been shown that, due to a combination of field-line sweep back and aberration, the phase of the center of the radio pulse ϕ_I should lead the phase of the max P.A. sweep rate by

$$\Delta\phi_{P.A.} \approx 4h_{LC} \qquad (7)$$

(e.g., Blaskiewicz et al. 1991; Dyks 2008). Observationally, we identify ϕ_I with the midpoint of the pulse at 10% of its peak

and $\phi_{\mathrm{P.A.}}$ is identified with ϕ_0 in an RVM fit. The true phase of minimum magnetic angle is between ϕ_I and $\phi_{d\psi,\max}$. These expressions assume simple static dipoles and low altitudes. We have checked against detailed numerical simulations of swept-back dipole magnetospheres and find that the actual pulse intensity center and phase of maximum P.A. sweep are both sensitive to details of the magnetic field structure, especially conditions at the light cylinder that define the edge of the open zone (Craig et al. 2011). These differences are modest at $h_{\mathrm{LC}} < 0.05$. For objects indicating higher altitude radio emission detailed comparison with the numerical results can be important.

In practice, radio pulse profiles may represent "patchy" illumination of the radio zone (Lyne & Manchester 1988), even for these young pulsars. This complicates our estimates of W and ϕ_I. In Table 1, we list both W_{10}, the full width of the radio pulse at 10% of the peak intensity and W_1, an estimate of the pulse width at 1% of the peak. These measurements were made on archival 1.4 GHz profiles (see table references). The W_1 estimate is necessarily approximate, especially for the lower signal-to-noise ratio (S/N) pulse profiles. At such low flux levels, extended pulsed emission may be generated by interstellar scattering tails, weak emission components unassociated with the main dipole cap or even nonlinearities in the measurement system. Nevertheless, for at least a few of these pulsars, this broader width captures weak components of the pulse coming from the principal emission zone. Further, in some cases, the assumption of pure dipole geometry and even the identification of the radio beam with the open zone are suspect. However, despite all of these caveats, these radio measurements do provide some phenomenological constraints on the range of allowable α and ζ, even when values for individual pulsars are suspect.

3.2. PWN Torus Fits

When the pulsar wind momentum is equatorially concentrated, one may observe a "torus" of emission at the spin equator, as for the Crab and Vela pulsars. The most useful examples are found in *Chandra* X-ray images of PWN tori, where synchrotron emission is produced in the mildly relativistic flow downstream from the termination shock. Doppler boosting allows one to distinguish the "front" and "back" sides and so fitting can measure the spin axis inclination to the line of sight (Ng & Romani 2008). The images are not, however, sensitive to the sign of the spin, so a torus fit cannot distinguish between ζ and $\zeta' = \pi - \zeta$. Occasionally, symmetric jets also allow ζ estimates. These fits provide relatively robust model-independent constraints on ζ, largely orthogonal to the RVM measurements, so that the combination provides a good picture of the pulsar geometry.

Unfortunately, to date no strongly "sub-luminous" pulsar has an X-ray torus measurement, since these are typically available only for very young $\tau < 10^{4.5}$ yr pulsars. However, PSR J1930+1852 (unseen by the LAT) has a fit angle $\zeta = 33 \pm 3°$ suggesting that its OG emission should not be visible (Ng & Romani 2008); as the LAT exposure increases this can eventually be a useful comparison. Also there is some hope of obtaining ζ estimates for older (even millisecond) pulsars from fits to the geometry of Hα bow shocks; in some cases (e.g., Romani et al. 2010, J1741−2054) these show clear signs of equatorially concentrated momentum flux and thus opportunities to constrain ζ.
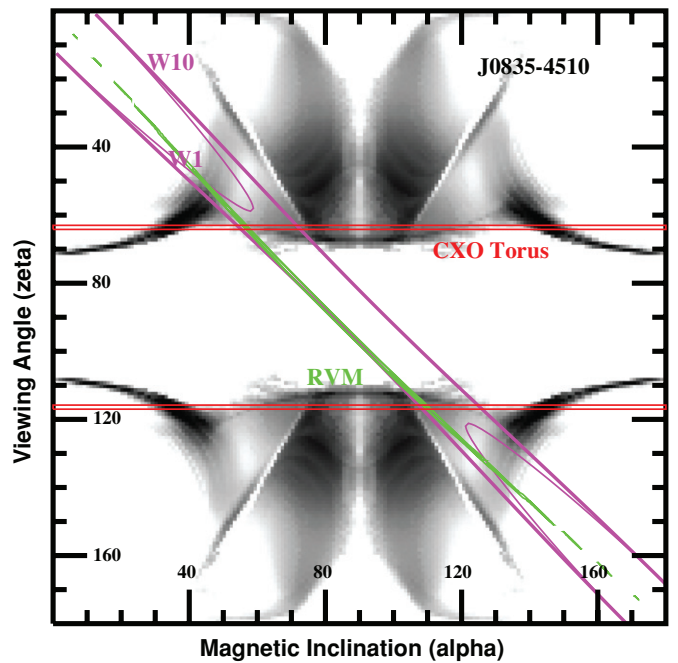

Figure 2. Spin geometry plane for Vela, with various observational constraints. The background gray scale shows the goodness of fit of the LAT light curve to a basic OG model, with dark colors better agreement.

(A color version of this figure is available in the online journal.)

4. INDIVIDUAL OBJECTS

We can combine these various geometry constraints to restrict the viable location of a pulsar in the (α, ζ) plane and for this location compare with the predictions of the various γ-ray emission models. As an example, we show in Figure 2 the constraints for the bright, well-studied Vela pulsar PSR J0835−4510 (B0833−45). The RVM model was originally developed for Vela (Radhakrishnan & Cooke 1969) so it is not surprising that the high S/N Vela data provides good constraints on β. As usual α is not well determined. However, there is a good measurement of ζ from *Chandra* images of the X-ray torus (Ng & Romani 2008). Finally, the pulse width constraints are shown. The background gray scale shows the "goodness of fit" of the LAT Vela profile to an OG light curve computed for the particular α and ζ, assuming a current-free retarded dipole field structure (RW10).

The contours marked RVM are quite crowded, since the high S/N Vela data provide very strong β constraints. These cross the ζ constraints from the X-ray torus and the two constraints select solutions at $(\alpha, \zeta) = (56°, 63°5)$ and $(109°, 116°5)$. For the estimated $\Delta\phi_{\mathrm{P.A.}}$ and the resulting $h_{\mathrm{LC}} \approx 0.018$, the pulse width W_{10} is easily consistent with these solutions. They are not consistent with the W_1 width, but such a wider pulse could be easily accommodated if this faint emission comes from slightly higher altitudes. Indeed, evidence of variable pulse components and microstructure in the Vela pulse wings (Johnston et al. 2001) suggests such multi-altitude emission. The darker gray scales in the background show regions with good fits to the LAT light curve. Evidently, the best regions in this model are not at the RVM + PWN preferred positions. As shown in RW10, model perturbations such as magnetospheric currents can shift the locations of the best fits; for example, OG models with currents can produce reasonable agreement with the $(109°, 116°5)$ solution. However, other models remain viable. For example, the "Separatrix Layer" model of Bai &
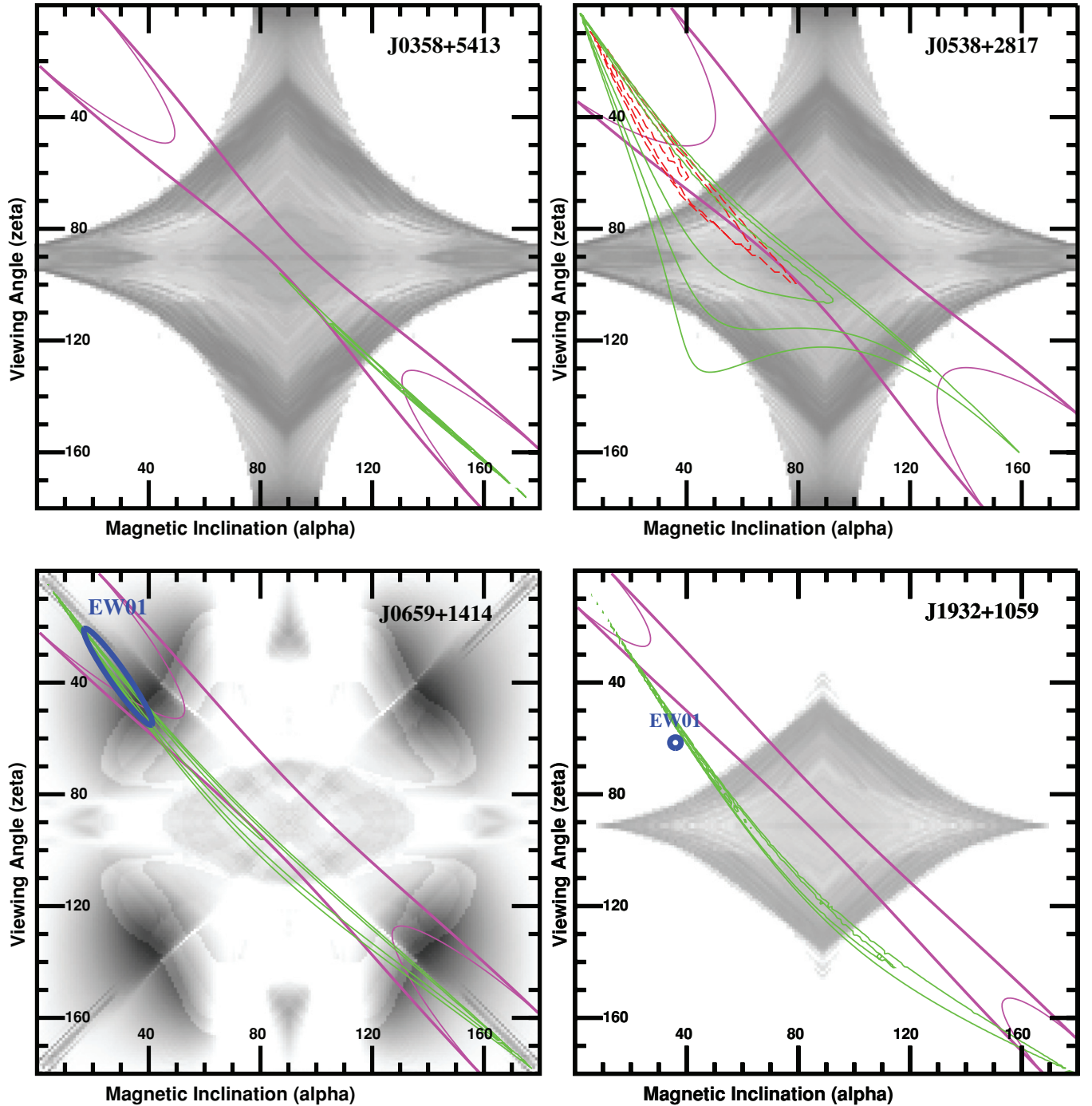
Figure 3. Spin geometry plane for sub-luminous pulsars with parallax distances. The backgrounds show the generic locations providing sharp OG pulses, except for PSR J0659+1414, where the background shows the allowed fits to the observed LAT pulses, including lower altitude (e.g., "two pole caustic" TPC) emission. Three green contours show the loci of best RVM matches, while the bold and narrow magenta curves showed the regions allowed by emission from the static dipole open zone for our estimated h_{LC}. For PSRs J0659+1414 (B0656+14) and J1932+1059 (B1929+10) the RVM fits of Everett & Weisberg (2001) are indicated. For PSR J0538+2817 the fits imply large h_{LC}, requiring a numerical magnetosphere model. The fits to the polarization geometry using such models are shown by the dashed (red) contours.

(A color version of this figure is available in the online journal.)

Spitkovsky (2010) produces a good match at the (56°, 63°.5) solution.

4.1. Pulsars with Parallaxes

In Figure 3, we show the constraints for the sub-luminous candidates having parallax measurements. The background gray scales show the region where a narrow OG, with gap widths

$w \approx L_{\gamma,\mathrm{heu}}/\dot{E}$, produces sharp caustic pulses. The gray levels indicate goodness of fit for a generic single γ-ray pulse. Of course with an actual LAT detection the detailed light curve and phase produce much more detailed constraints within this envelope (see Figure 2). Note that sharp OG pulses are not expected (white background) near the spin poles unless the pulsar is an orthogonal rotator. In contrast, lower altitude (e.g.,

two pole caustic (TPC)) models produce emission at small β all the way to the poles and good pulse matches are expected in the OG blank zones, if such low-altitude gaps are active.

PSR J0358+5413 (B0355+54) is a bright radio pulsar for which RVM fits provide good β constraints and a preference for $\alpha > 110°$. At the estimated $\Delta\phi_{\rm P.A.}$, the W_{10} pulse width does not significantly tighten this bound, but if we include the wider W_1 width the constraints tighten with $\alpha > 130°$ and $\zeta > 140°$. This is also the region of best RVM fits. Thus, while the best-fit geometry localizes to (α, ζ) where OG emission would not be visible, acceptable solutions include the range that could be consistent with visible high-altitude γ-rays. Since our present flux bound only restricts us to $< L_{\gamma,\rm heu}/3$ we regard this as a plausible sub-luminous pulsar, but not a strong case. Increased LAT exposure and improved geometrical constraints are needed to make this definitive.

PSR J0538+2817 in contrast has only rather poor RVM constraints. However, the large pulse width does help to restrict the range of viable solutions, even though $h_{\rm LC}$ is high. Here the best combined radio data seem to prefer small α and small ζ. In fact if the W_1 constraint is included we conclude $\alpha < 35°$ and $\zeta < 50°$ so we would not expect to see OG emission. However, using only the W_{10} width a wide range of α is allowed toward the edges of the RVM and pulse width contours. *Chandra* in fact shows a small X-ray PWN around the pulsar (Romani & Ng 2003; Ng et al. 2007). Unfortunately, the emission is too faint and compact to provide a good ζ measurement, although the existence of opposing jet-like features suggest $\zeta \approx 90°$. Interestingly, Kramer et al. (2003) find an RVM fit giving $\alpha \approx 85°$ and $\beta \approx -2°$, which would be consistent with jets viewed near side-on; however, this solution is well outside the RVM-allowed region in Figure 3. It is worth noting that with this pulsar's large $h_{\rm LC} = 0.14$ the detailed field treatment of Craig et al. (2011) can be important. The dashed (red) contours show the constraints from fits to these numerical models. The best-fit altitude depends on α and ζ, ranging from $h_{\rm LC} = 0.13–0.17$. The contours show best solutions to these numerical models, marginalized over $h_{\rm LC}$. Good solutions are found for $\alpha < 40°$, acceptable solutions are at $\alpha < 80°$. Again we must conclude that alignment is preferred, but nearly orthogonal rotators are not excluded. This is a case where improved radio observations with higher S/N can substantially improve the polarization modeling constraints.

The next object, **PSR J0659+1414** (B0656+14), is the archetype sub-luminous pulsar. This object was included in the very careful polarization study of Everett & Weisberg (2001), who found $\alpha = 29° \pm 23°$ and $\beta = 8°.9 \pm 6°.1$ (blue ellipse). Earlier, Lyne & Manchester (1988) found $\alpha \approx 8°.2$ and $\beta \approx 8°.2$, so there has been some consensus that this is an aligned pulsar. However, we and Weltevrede et al. (2010) find less strong constraints on α even though we are fitting the same 1.4 GHz data from long Arecibo integrations used in Everett & Weisberg (2001). In our case, the best fits slightly prefer small $\alpha < 80°$, although all values are allowed. However, PSR J0659+1414 has weak but well-measured emission extending well beyond the peak of the pulse, giving a large $W_1 = 54°$. Including this constraint does indeed prefer near alignment. Our best fits are in fact for $\alpha < 35°$ although the large $\alpha > 130°$ fits are nearly as good. As the background to the constraints in this panel we show the gray scale goodness of fit for the LAT data compared with a TPC model. This model includes emission from below the null charge surface and so predicts gamma-ray detections all the way to the spin axis. There are in fact two broad zones of

reasonable TPC model fits consistent with the radio constraints near $\alpha \approx 40°$ and $\alpha \approx 140°$. In contrast the OG model for this pulsar's $\dot{E}$ has no γ-ray emission for solutions at $\alpha < 50°$ or $\alpha > 130°$. Thus, *if* we adopt both the RVM and pulse width constraints, a large fraction of the remaining phase space is incompatible with γ-ray emission from an OG model and a lower altitude (e.g., TPC-type) component is preferred. If we adopt the W1 constraint or the Everett & Weisberg (2001) α value, this becomes a strong conclusion. However, with the less strict angle constraints inferred in this paper, OG exclusion is suggested, not required.

The final parallax candidate is **PSR J1932+1059** (B1929+10), which has lower $\dot{E}$ than the cuts for our uniform sample. This pulsar has been the subject of many polarization studies, summarized in Everett & Weisberg (2001), who find $\alpha = 35°.97 \pm 0°.95$, $\zeta = 61°.52 \pm 1°.3$ from a fit excluding the main pulse, with the high S/N leading to very small statistical errors (blue circle). For consistency with the other objects in this paper, we have fit the main peak width and P.A. sweep. Our RVM fit prefers $\alpha < 60°$, close to the EW01 value, while allowing all α, as usual. However, given the large pulse width and low $h_{\rm LC}$ of Table 1, nearly aligned rotators are preferred. For the W_{10} width we infer $\alpha < 20°$, while the W_1 width implies $\alpha < 15°$. The situation for this pulsar is not clear; these pulse width constraints are not consistent with the EW01 fit. Moreover, this pulsar has a widely separated faint pulse component which would be identified as an interpulse for orthogonal solutions, but for more aligned solutions suggests a very wide pulse profile. Such emission can only come from the open zone for very large $h_{\rm LC}$, which we do not model here. Nevertheless, for either the EW01 solution or the RVM/pulse width constraints, high-altitude γ-ray emission is not expected to be visible at Earth for this small $\dot{E}$ pulsar. At first sight this would seem to provide a strong confirmation of the connection between alignment and low γ-ray flux. However, with such a low $\dot{E}$, this pulsar is in the "death zone" where powerful γ-ray gap emission may have turned off.

4.2. Sub-luminous Candidates without Parallaxes

Since the objects with precise distances do not yet provide a definitive test of the nature of sub-luminous pulsars, we check other pulsars for which the LAT provides relatively low luminosities at their estimated distances. For example, **PSR J0745−5353** (B0743−53) is assigned a distance of 0.25 kpc in the CL02 model, because it is superimposed on H II emission associated with the Gum nebula. At this distance the flux is $>450\times$ less than that expected from $L_{\gamma,\rm heu}$. However, at the 7.1 kpc distance implied by the Taylor & Cordes (1993) model the upper limit is not constraining (the pulsar does remain sub-luminous for distances as large as 2 kpc). The combined RVM and pulse width constraints imply $\alpha > 150°$ (W_{10}) or $\alpha > 160°$ (W_1). Clearly, these constraints indicate an anti-aligned rotator such that only γ-ray emission from below the null charge surface ($r < r_{\rm NC}$) should be visible. Unfortunately, the highly uncertain distance prevents us from drawing strong conclusions from the absence of flux from this pulsar. A parallax distance measurement (or at least a lower limit) would be of particular value; if a low distance is confirmed it provides a sharp test of the γ-ray beaming geometry.

Our final pulsar is **PSR J1740+1000**. This pulsar is of interest since it is young and is located well off the Galactic plane. This makes for a very clean LAT flux limit and a relatively robust DM distance. We have performed RVM fits using polarization
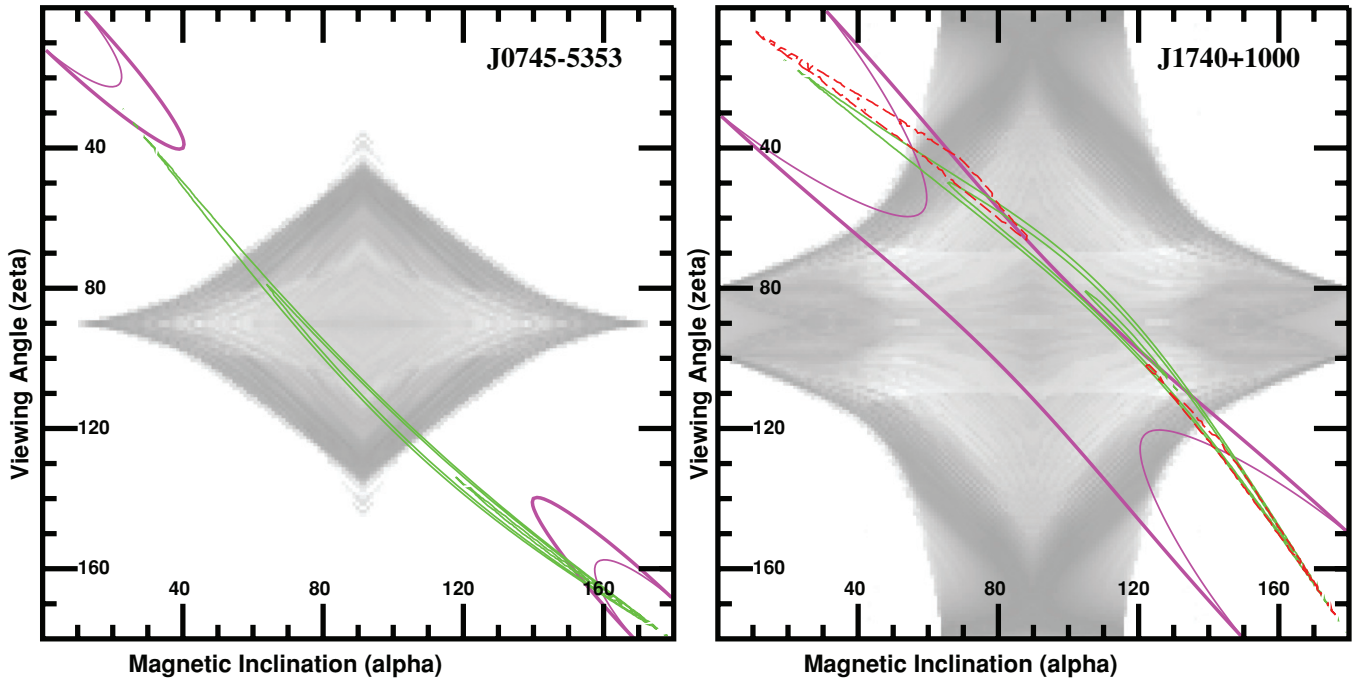
Figure 4. Spin geometry plane for two pulsars without parallax distances, showing the radio polarization and pulse width constraints. For geometries away from the gray background, the sources are not expected to have strong outer magnetosphere γ-ray pulses. The PSR J1740+1000 data suggest large h_{LC} requiring numerical modeling; the locus of best fits for these models is shown by the dashed (red) contours.

(A color version of this figure is available in the online journal.)

data collected at Nançay with the Berkeley–Orléans–Nançay (BON) pulsar back end (see Theureau et al. 2011). The fits allow a large α range, but prefer values near 120°. However, such an orthogonal rotator is very difficult to accommodate with the very wide observed pulse, even for the relatively large $h_{LC} = 0.122$ inferred here from $\Delta\phi_{P.A.}$. The standard pulse width constraints are shown in Figure 4; to accommodate the W_{10} width implies $\alpha < 70°$ or $> 120°$, while the W_1 width requires $\alpha < 50°$ or $> 140°$. Interestingly, if we fit the numerical magnetosphere models, the large α solution becomes preferable and in fact shifts to slightly higher values. The red (dashed) contours show the numerical model fit including Ψ points within W_{10}. For numerical fits placing points out to the W_1 pulse width in the open zone, the allowed region moves inside the magenta W_1 contour and we find $\alpha \approx 30°$ or $150°$, where one would expect no high-altitude γ-ray emission at this $\dot{E}$. However, if we only consider the data within the W_{10} pulse width an appreciable region including OG-type emission is allowed. Thus, the geometry of this pulsar is not yet sufficiently constrained to test the models. Improved orientation constraints, perhaps from additional radio and X-ray observations, are needed. A parallax measurement would also be very valuable for strengthening the use of this pulsar to test luminosity models.

4.3. Other Nearby, Energetic Radio Pulsars

The DM-distance cut selects three additional young energetic radio pulsars, but these, plotted on Figure 1 (right), may well have typical LAT pulsar luminosities. First, PSR J0834−4159 is undetected with a flux limit giving $\sim 1/3\, L_{\gamma,\mathrm{heu}}$ at its DM distance. Like J0745−5353, this pulsar's DM distance estimate is dramatically smaller in the CL02 model (1.6 kpc) than in the Taylor & Cordes (1993) TC93 model (9.7 kpc), due to inclusion of nearby H II complexes. However, unlike J0745−5353, even a

modest factor of 2 increase in the true distance would make the present flux bound unconstraining. Geometrical data on this pulsar are limited. It has pulse components separated by $\approx 165°$, so it is a likely interpulsar (Weltevrede & Johnston 2008). However, unlike other pulsars discussed in this paper it has very little linear polarization, so the geometry has not been confirmed by RVM modeling. In sum, this is not a strong case for a sub-luminous pulsar. Indeed, the limited radio information suggests a near-orthogonal rotator and thus γ emission beamed toward Earth. Continued LAT exposure and improved radio data can help to clarify the situation.

Statistically significant LAT flux is found in the direction of PSR J0857−4424. Like the other pulsars in this region, the DM-estimated distance had a major adjustment and should be considered uncertain. In addition, background systematics can perturb the LAT flux estimate. We conclude that this pulsar is likely not sub-luminous, although a LAT pulsed detection is required for firm conclusions. Unfortunately, the lack of significant linear polarization in this pulsar will make it very difficult to extract detailed radio geometry constraints.

The last nearby energetic object is PSR J1722−3712 (B1719−37) at 1.9 kpc (CL02). This interpulsar has been the subject of a very careful polarization study by Keith et al. (2010) who find (EW01-corrected) angles $\alpha = 89°.3 \pm 0°.1$ and $\zeta = 83°.9 \pm 0°.3$. Thus, we have high confidence that this is an orthogonal rotator and we expect to see visible OG emission. The LAT does, in fact, provide an unpulsed detection. There are no particular issues with DM in this direction and the LAT detection is consistent with a point source, localized to the radio pulsar position and having a pulsar-like γ-ray spectrum. The inferred luminosity is quite consistent with $L_{\gamma,\mathrm{heu}}$. Thus, this object has a well-constrained geometry indicating that the outer magnetosphere γ-ray beams should be visible and we do indeed detect the source. Interestingly, of the five $d < 3$ kpc interpulsars

in the study of Keith et al. (2010) three are LAT detected (PSR J1057−5226 = B1055−52 at 0.7 kpc, PSR J1722−3712 = B1719−37 at 1.9 kpc and PSR J0908−4913 = B0906−49 at 2.5 kpc) while the other two (PSR J1549−4848 at 2.7 kpc and PSR J1739−2903 = B1736−29 at 2.5 kpc) have at present high upper limits or weak detections, quite consistent with $L_{\gamma,\mathrm{heu}}$.

LAT pulse searches for these objects and similar interpulsars with well-constrained geometries can provide important model tests. Note that with $\zeta \approx 90°$ we are probing emission very near the null charge surface for these objects. As it happens, the presence of γ-ray OG emission in this region is sensitive to the magnetospheric currents (Hirotani 2006). The shape and phase of the LAT pulsations allow us to trace the emission to particular magnetosphere zones. When kinematic distances are also available, we then have the actual luminosity of these zones, a particularly powerful model constraint. Unfortunately, such constraints are very difficult to obtain for the nearly aligned pulsars which are plausibly associated with the sub-luminous pulsar class discussed here.

5. CONCLUSIONS AND FUTURE PROSPECTS

We have examined the set of 12 young, energetic radio pulsars with $d \leqslant 2$ kpc. Most follow the standard LAT pattern of powerful, efficient high-altitude γ-ray emission with luminosity $\sim L_{\gamma,\mathrm{heu}}$. However PSR J0659+1414, at 1/20th of this luminosity, is a clear outlier. Present flux bounds make a good case that PSR J0538+2817 is also $\sim 10\times$ sub-luminous. Although they lack parallaxes, PSRs J0745−5353 and J1740+1000 are also likely to produce $< 0.1 L_{\gamma,\mathrm{heu}}$. PSR J0358+5413 has a parallax, but a less restrictive bound, at present. Thus, we find that four and perhaps five of our nearby energetic sample may be members of this sub-luminous class, although for several of these pulsars the case could be strengthened with parallax distance measurements.

We have attempted to determine whether this may be attributed to beaming away from Earth, as would be expected for high-altitude (OG) emission and aligned or anti-aligned spin geometries. Unfortunately, precise geometrical constraints are very difficult to obtain for aligned rotators. We do find that for our sub-luminous pulsar candidates the present radio constraints prefer aligned geometries. The best cases are probably PSR J0538+2817 and PSR J0745−5353. Although it lies below the $\dot{E}$ cut for our sample set, PSR J1932+1059 also seems sub-luminous and aligned. However, no one case for alignment is compelling.

The converse argument is in somewhat better shape. When we know that the pulsar is orthogonal, we seem to see γ-ray emission at the expected $L_{\gamma,\mathrm{heu}}$. PSR J1722−3712 is an excellent example. Although the undetected PSR J0834−4159 may be orthogonal, its distance estimate is particularly uncertain, and its present flux limit is quite likely compatible with $L_{\gamma,\mathrm{heu}}$.

In the population synthesis of Watters & Romani (2011) it was concluded that for OG geometries $\approx 30\%$ of the radio-selected $\log(\dot{E}) > 33.5$ pulsars should be undetected in the γ-rays, simply due to beaming. Our present sub-luminous pulsar fraction, (4 to 5)/12 pulsars, is consistent with this ratio, given the small number statistics. However, we would not expect many more sub-luminous pulsars unless the radio beams are substantially larger than and/or γ-ray beams are substantially smaller than assumed in these beaming computations. The fact that we see evidence for high-altitude ($h_{\mathrm{LC}} > 0.1$) radio emission in several of our pulsars supports the presence of

wide radio beams and a somewhat larger sub-luminous pulsar fraction; Ravi et al. (2010) have also argued that the statistics of radio and γ-ray detections imply wide radio beams for young pulsars.

The *detection* of PSR J0659+1414 at $\sim L_{\gamma,\mathrm{heu}}/20$ presents an important addition to this beaming picture. This low-flux level, together with the γ-ray pulse's unusual phase and soft spectrum suggest atypical magnetospheric emission. If this is an aligned (or anti-aligned) rotator, this must be low-altitude $r < r_{\mathrm{NC}}$ emission. A set of J0659+1414 type pulsars is certainly needed to probe the origin of this low flux.

If we assume that several of our sub-luminous candidates join the J0659+1414 class, we already have hints to the common features. Certainly non-orthogonal geometries seem preferred, although better geometrical constraints are needed for most sources to establish them as aligned rotators. Other plausible peculiarities for PSR J0659+1414 exist; for example, it has the lowest light cylinder field B_{LC} of any LAT radio pulsar. Table 1 lists B_{LC} for our candidates. No strong trend is evident, and certainly the few kG fields of PSRs J0358+5413, J0538+2817, and J1740+1000 are quite typical of those of detected LAT pulsars. For these objects, at least, orientation seems more promising.

Since several of our sub-luminous candidates have limits on luminosity approaching the J0659+1414 level, it will be important to see if increased LAT exposure or pulsed searches can detect evidence of similar low-level γ-ray emission. Any such pulse detections for these sources must then represent an atypical "sub-luminous" mechanism. The phasing of such pulses can be used to cement the geometrical location and their spectrum and dependence on spin properties should help lock down the emission physics. The prospect of using the LAT to probe a second domain of pulsar particle acceleration, in addition to the established high-luminosity outer magnetosphere emitters, is very exciting.

REFERENCES

Abdo, A. A., Ackermann, M., Ajello, M., et al. 2009, Science, 325, 840
Abdo, A. A., Ackermann, M., Ajello, M., et al. 2010a, ApJS, 187, 460
Abdo, A. A., Ackermann, M., Ajello, M., et al. 2010b, ApJS, 188, 405
Arons, J. 1996, A&AS, 120, 49
Bai, X.-N., & Spitkosky, A. 2010, ApJ, 715, 1282
Blaskiewicz, M., Cordes, J. M., & Wasserman, I. 1991, ApJ, 370, 643
Cordes, J. M., & Lazio, T. J. W. 2002, arXiv:astroph/0207156
Craig, H., Romani, R. W., & Johnston, S. 2011, BAAS, 43, 336.02
Deller, A. T. 2009, PhD thesis, Swineburne Univ., Melbourne
Dyks, J. 2008, MNRAS, 391, 859
Everett, J. E., & Weisberg, J. M. 2001, ApJ, 553, 341
Gould, D. M., & Lyne, A. G. 1998, MNRAS, 301, 235
Harding, A. K. 1981, ApJ, 245, 267
Hirotani, K. 2006, ApJ, 652, 1475
Johnston, S., Hobbs, G., Vigeland, S., et al. 2005, MNRAS, 364, 1397
Johnston, S., van Straten, W., Kramer, M., & Bailes, M. 2001, ApJ, 549, L101
Karastergiou, A., & Johnston, S. 2007, MNRAS, 380, 1678
Keith, M., Johnston, S., Weltevrede, P., & Kramer, M. 2010, MNRAS, 402, 745
Kerr, M. 2010, PhD thesis, Univ. Washington, Seattle, WA
Kramer, M., Lyne, A. G., Hobbs, G., et al. 2003, ApJ, 593, L31
Lyne, A. G., & Manchester, R. N. 1988, MNRAS, 234, 477
Manchester, R. N., Hobbs, G. B., Teoh, A., & Hobbs, M. 2005, AJ, 129, 1993
Ng, C.-Y., & Romani, R. 2008, ApJ, 673, 411
Ng, C.-Y., Romani, R. W., Brisken, W. F., Chatterjee, S., & Kramer, M. 2007, ApJ, 654, 487
Noutsos, A., Abdo, A. A., Ackermann, M., et al. 2011, ApJ, 728, 77
Radhakrishnan, V., & Cooke, D. J. 1969, ApL, 3, 225
Ravi, V., Manchester, R. N., & Hobbs, G. 2010, ApJ, 716, l85
Romani, R., & Ng, C.-Y. 2003, ApJ, 585, L41
Romani, R. W., Shaw, M. S., Camilo, F., Cotter, G., & Sivakoff, G. R. 2010, ApJ, 742, 908
Romani, R., & Watters, K. P. 2010, ApJ, 714, 810 (RW10)
Saz Parkinson, P. M., Dormody, M., Ziegler, M., et al. 2010, ApJ, 725, 571
Taylor, J. H., & Cordes, J. M. 1993, ApJ, 411, 674
Theureau, G., Parent, D., Cognard, I., et al. 2011, A&A, 525, 94
von Hoensbroech, A., & Xilouris, K. M. 1997, A&AS, 126, 121
Watters, K. P., & Romani, R. W. 2011, ApJ, 727, 123
Watters, K. P., Romani, R. W., Weltevrede, P., & Johnston, S. 2009, ApJ, 695, 1289
Weltevrede, P., Abdo, A. A., Ackermann, M., et al. 2010, ApJ, 708, 1426
Weltevrede, P., & Johnston, S. 2008, MNRAS, 387, 1755